HEALTH AND MEDICINE

Cryo-shocked tumor cells deliver CRISPR-Cas9 for lung cancer regression by synthetic lethality

Feng Liu[1,2]†, Minhang Xin[1]†, Huiheng Feng[1,2], Wentao Zhang[1], Ziyan Liao[1,2], Tao Sheng[1], Ping Wen[1,2], Qing Wu[1,2], Tingxizi Liang[1,2], Jiaqi Shi[1,2], Ruyi Zhou[1], Kaixin He[1,3]*, Zhen Gu[1,2,3,4,5,6]*, Hongjun Li[1,2,3,4,7]*

Although CRISPR-mediated genome editing holds promise for cancer therapy, inadequate tumor targeting and potential off-target side effects hamper its outcomes. In this study, we present a strategy using cryo-shocked lung tumor cells as a CRISPR-Cas9 delivery system for cyclin-dependent kinase 4 (*CDK4*) gene editing, which initiates synthetic lethal in KRAS-mutant non–small cell lung cancer (NSCLC). By rapidly liquid nitrogen shocking, we effectively eliminate the pathogenicity of tumor cells while preserving their structure and surface receptor activity. This delivery system enables the loaded CRISPR-Cas9 to efficiently target to lung through the capture in pulmonary capillaries and interactions with endothelial cells. In a NSCLC-bearing mouse model, the drug accumulation is increased nearly fourfold in lung, and intratumoral CDK4 expression is substantially down-regulated compared to CRISPR-Cas9 lipofectamine nanoparticles administration. Furthermore, CRISPR-Cas9 editing–mediated CDK4 ablation triggers synthetic lethal in KRAS-mutant NSCLC and prolongs the survival of mice.

INTRODUCTION

The incidence of lung cancer remains the primary contributor to global mortality rates associated with cancer, resulting in an estimated 1.8 million fatalities annually (*1*, *2*). Among the different histological subtypes, non–small cell lung cancer (NSCLC) accounts for about 85% of cases (*3*, *4*). Unfortunately, for the majority of patients suffering from advanced or metastatic NSCLC, as well as those without specific therapeutic targets, the median overall survival remains low even despite the integration of now accessible treatments (*2*, *5*–*7*). As a promising gene editing tool, CRISPR-Cas9 harbors the potential for the diagnosis and treatment of various tumors, virus infections, and genetic disorders (*8*–*11*). Unlike traditional therapies, CRISPR-Cas9 presents a distinct advantage by permanently disrupting genes crucial for tumor survival, thus bypassing the requirement for repetitive dosing (*12*, *13*). However, there are challenges that impede the clinical application of CRISPR-Cas9, such as its degradation or denaturation in the bloodstream and low efficiency of delivery (*14*, *15*). In addition, the prominent vectors for CRISPR-Cas9 delivery, viral and nonviral, lack tissue-targeting capabilities and cell selectivity, presenting a critical hurdle for the in vivo application of CRISPR therapy (*16*–*18*).

Here, we report a lung-targeted CRISPR-Cas9 drug delivery strategy based on passive and active dual-targeting for knocking down cyclin-dependent kinase 4 (*CDK4*) in tumors to induce synthetic lethality in NSCLC (Fig. 1A). Synthetic lethality is defined as the simultaneous inactivation of two genes leading to cell death, and the individual functional loss has little impact on cell viability (*19*, *20*). In general, tumor cells harbor oncogene mutations, rendering them become more addiction to some certain genes for maintaining cellular homeostasis (*21*). In principle, these tumor cells that carry the specific mutation can be selectively killed by pharmacologically inhibiting another gene with a synthetic lethal interaction, while normal cells can be spared the effects of the drugs due to lacking the specific genetic alteration (*21*, *22*). Therefore, synthetic lethality provides a promising therapeutic strategy for targeting undruggable oncogenes while attenuating damage to normal tissues and cells (*23*, *24*). So far, some synthetic lethal interactions have been applied in clinical trials and therapies (*25*, *26*). In NSCLC, kirsten rat sarcoma virus (*KRAS*) oncogene mutations dominate more than 25% of the distinct biological and clinical subtypes (*27*, *28*). Recently, several synthetic lethal interactions have been identified in KRAS-mutant NSCLC (*29*–*31*), providing an alternative way to potentiate the clinical benefits. A549 cell is a typical KRAS-mutant NSCLC cell. Following rapid cryo-inactivation with liquid nitrogen treatment (LNT) as well as elimination of pathogenicity, it is used here as a vector for in vivo CRISPR-Cas9 delivering. Benefiting from the intact cellular architecture and preserved cell surface glycoprotein, CD44, this cell vehicle enables highly targeted lung delivery through passive trapping by lung capillaries, as well as cell interaction and adhesion mediated by CD44. The pCas9/gCDK4 plasmids, utilized for CDK4 ablation, is coassembled with a typical transfection reagent, lipofectamine 3000, to form nanoformulation and anchored to the surface of LNT cells by electrostatic interactions. CDK4 ablation could induce the death of NSCLC cells carrying KRAS mutations but did not lead to dysfunction of normal cells.

RESULTS

Characterization of LNT A549 cells

Liquid nitrogen–treated human NSCLC cells were prepared according to the previous literature (*32*, *33*). To assess the morphology after

[1]National Key Laboratory of Advanced Drug Delivery and Release Systems, College of Pharmaceutical Sciences, Zhejiang University, Hangzhou 310058, China. [2]Liangzhu Laboratory, Zhejiang University, Hangzhou 311121, China. [3]Jinhua Institute of Zhejiang University, Jinhua 321299, China. [4]Key Laboratory of Advanced Drug Delivery Systems of Zhejiang Province, College of Pharmaceutical Sciences, Zhejiang University, Hangzhou 310058, China. [5]Department of General Surgery, Sir Run Run Shaw Hospital, School of Medicine, Zhejiang University, Hangzhou 310016, China. [6]MOE Key Laboratory of Macromolecular Synthesis and Functionalization, Department of Polymer Science and Engineering, Zhejiang University, Hangzhou 310027, China. [7]Department of Hepatobiliary and Pancreatic Surgery the Second Affiliated Hospital, School of Medicine, Zhejiang University, Hangzhou 310009, China.
*Corresponding author. Email: hekaixin@zju.edu.cn (K.H.); guzhen@zju.edu.cn (Z.G.); hongjun@zju.edu.cn (H.L.)
†These authors contributed equally to this work.

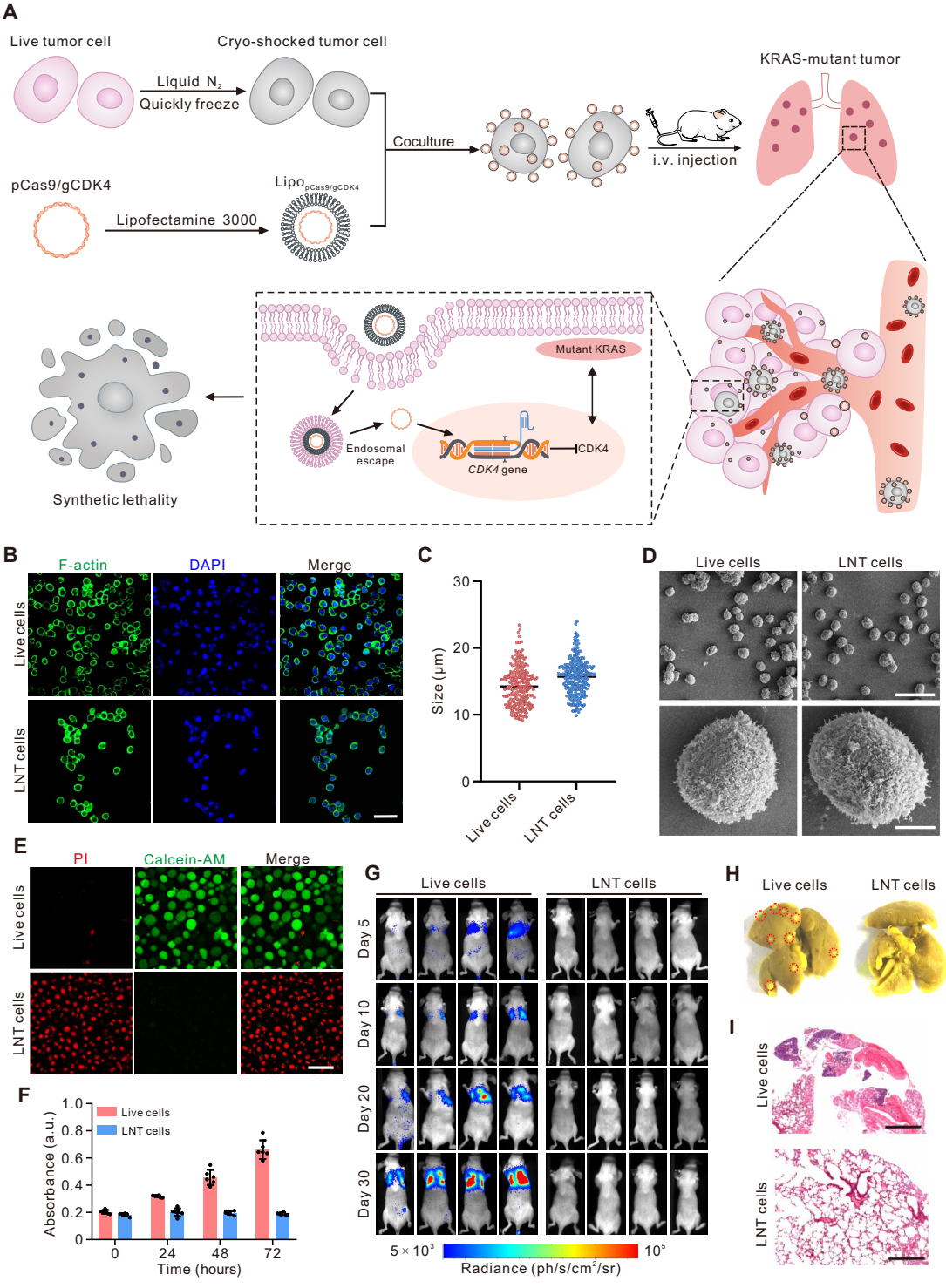

Fig. 1. Characterization of LNT cells. (**A**) Schedule of LNT cells delivery of CRISPR-Cas9 nanoparticles for KRAS-mutant NSCLC treatment. (**B**) Representative cell structure images of LNT and live A549 cells. F-actin was stained with phalloidin-488 and nucleus was labeled with 4′,6-diamidino-2-phenylindole (DAPI). Scale bar, 50 μm. (**C**) Size statistics of live and LNT A549 cells, $n = 252$. (**D**) Representative SEM images of live and LNT A549 cells. Scale bars, 50 μm (top) and 5 μm (bottom). (**E**) Representative images of LNT and live A549 cells stained with calcein-AM (live cells) and propidium iodide (dead cells). Scale bar, 50 μm. (**F**) CCK8 assay of live and LNT A549 cells after culturing for different times, $n = 6$. (**G**) The in vivo bioluminescence signals after injection with luciferase transfected live and LNT A549 cells, $n = 4$. (**H**) Representative lung photographs after intravenous injection with live and LNT A549 cells for 30 days; red dotted circle marked tumors. (**I**) Representative hematoxylin and eosin (H&E) staining of lung tumor lesions. Scale bars, 300 μm. All data are presented as means ± SD. i.v., intravenous; a.u., arbitrary units.

liquid nitrogen treatment, we labeled the cytoskeleton in LNT A549 cells with phalloidine. Confocal microscopy analysis showed that LNT cells (~15.3 μm) exhibited a comparable cellular structure as live cells (~14.7 μm) with a similar average size (Fig. 1, B and C). The morphology of LNT cells was also shown in the scanning electron microscopy (SEM) images. LNT cells presented a spherical structure with a similar rough surface compared with live cells, indicating that liquid nitrogen cryo-shocked NSCLC cells preserved the structure of live cells (Fig. 1D). To investigate whether LNT cells hold functional protein, SDS–polyacrylamide gel electrophoresis assay was executed and showed that A549 LNT cells retained almost all of the protein expressed in live A549 cells (fig. S1A). Furthermore, the Western blot and immunofluorescence staining demonstrated a high expression of CD44, an important protein expressed on the membrane of tumor cells, participating in cell-cell interaction and adhesion (*34*, *35*), on the LNT cells (fig. S1, B and C).

To further explore the LNT cell viability, we performed Live/Dead staining with calcein acetoxymethyl ester (calcein-AM) and propidium iodide (PI) to label live cells and dead cells, respectively. As shown in Fig. 1E, almost all of the live cells presented green fluorescence (calcein-AM), whereas all LNT cells gave out red signals (PI). Furthermore, we cultured LNT cells and live cells for 3 days and evaluated the cell viability by cell counting kit 8 assay (CCK8). An obvious viability increase (threefold) was found in live A549 cells after 3 days of cultivation; by contrast, there was no change in absorption value at 450 nm in LNT cells within 3 days (Fig. 1F). To further explore the pathogenicity of LNT cells, we administrated the cryo-shocked and live A549 cells into mice by intravenous injection and continuously monitored the oncogenesis. As shown in Fig. 1G, we found that live A549 cells exhibited rapid proliferation in vivo, as demonstrated with strong bioluminescence, while there was no detectable bioluminescence signal in the mice receiving A549 LNT cell injection at day 30. Moreover, the lungs from mice injected with live cell showed pulmonary tumor nodules (red dashed border) and obvious bioluminescence signals. By contrast, no microtumors could be found in the lungs of mice injected with A549 LNT cells (Fig. 1, H and I, and fig. S2). These results indicate that cryo-shocked A549 cells exhibit biosafety in vitro and in vivo.

Leveraging LNT cells as the targeting gene carrier

CRISPR-Cas9 genome editing system exhibits the potential for tumor therapeutics (*36*, *37*). To start with, we prepared lipofectamine encapsulating CRISPR-Cas9 plasmid for specific knockout of *CDK4*, a vital regulator in KRAS-mutant NSCLCs. A transmission electron microscope image revealed that the lipofectamine encapsulating CRISPR-Cas9 ($Lipo_{pCas9/gCDK4}$) nanoparticles had a diameter range from 100 to 400 nm (Fig. 2A). Furthermore, the size and zeta potential of the $Lipo_{pCas9/gCDK4}$ was 294 nm and 40.8 mV, respectively (Fig. 2B). In addition, the polymer dispersity index was 0.177, suggesting that $Lipo_{pCas9/gCDK4}$ nanoparticles were uniform (fig. S3). Next, we labeled pCas9/gCDK4 plasmid with iFluor 647 by covalent linkage and anchored the $Lipo_{pCas9/gCDK4}$ nanoparticles onto the surface of LNT A549 cells by electrostatic interactions between cationic liposomes and membrane phospholipids. Confocal microscopy imaging revealed that $Lipo_{pCas9/gCDK4}$ nanoparticles were distributed on the surface of cryo-shocked A549 cells (Fig. 2C). When incubating the $Lipo_{pCas9/gCDK4}$ nanoparticles with 2.5×10^6 LNT cells for 1 hour, we found that more than 85% $Lipo_{pCas9/gCDK4}$ nanoparticles anchored on the LNT cells (fig. S4A). Furthermore, a sustained release of pCas9/gCDK4 nanoparticles from the drug-loaded LNT cells ($LNT@Lipo_{pCas9/gCDK4}$) was detected, and approximately 78% of pCas9/gCDK4 was released within 10 hours (fig. S4B).

To enhance CRISPR-Cas9 gene editing efficiency, $Lipo_{pCas9/gCDK4}$ nanoparticles, released by LNT cells, must escape from lysosomes and translocate into cytoplasm. We assessed their ability to escape from lysosomes through subcellular localization studies. For better visual observation of $LNT@Lipo_{pCas9/gCDK4}$ colocalization with lysosomes, we cocultured A549 cells with $LNT@Lipo_{pCas9/gCDK4}$ containing iFluor 647–labeled pCas9/gCDK4 plasmid. Confocal imaging revealed that only a few $Lipo_{pCas9/gCDK4}$ nanoparticles entered the cells within 2 hours, owing to the possibility that the nanoparticles had not yet peeled off from the LNT cell membrane (fig. S5). At 6 hours, we found that remarkable red fluorescence puncta localized within green regions (lysosome), which suggested that some $Lipo_{pCas9/gCDK4}$ nanoparticles were engulfed by tumor cells and wrapped in lysosomes. Moreover, an obvious reduction in colocalization of lysosome and $Lipo_{pCas9/gCDK4}$ nanoparticles at 12 hours implied that a considerable portion of $Lipo_{pCas9/gCDK4}$ nanoparticles escaped from lysosomes (Fig. 2D).

Synthetic lethal efficiency of $LNT@Lipo_{pCas9/gCDK4}$

High CDK4 expression is closely related to KRAS-mutant NSCLCs tumor progression, which reveals the synthetic lethal interaction between KRAS and CDK4 (*29*). To determine the efficacy of gene editing of $LNT@Lipo_{pCas9/gCDK4}$, we investigated the expression of CDK4 via coculturing A549 cells with $LNT@Lipo_{pCas9/gCDK4}$ for 36 hours. Western blot assay revealed a down-regulation of CDK4 in $Lipo_{pCas9/gCDK4}$ and $LNT@Lipo_{pCas9/gCDK4}$ groups, respectively, while LNT cells and free plasmid showed no decrease (Fig. 3, A and B). Moreover, to explore the regulation of $LNT@Lipo_{pCas9/gCDK4}$ on CDK4 in the tumor cells that carry non-KRAS mutation, we chose human lung squamous cell carcinoma H226 cells as a wild-type KRAS candidate. Similarly, both $Lipo_{pCas9/gCDK4}$ and $LNT@Lipo_{pCas9/gCDK4}$ induced the decrease of CDK4 expression in H226 cells, respectively (Fig. 3, C and D). In addition, immunofluorescent staining of the A549 cells treated with $LNT@Lipo_{pCas9/gCDK4}$ showed an obvious down-regulation of CDK4 expression (Fig. 3, E and F).

To test whether CDK4 knockdown causes synthetic lethality in KRAS-mutant NSCLC cells, we cocultured A549 cells with $LNT@Lipo_{pCas9/gCDK4}$ and conducted CCK8 analysis. As shown in Fig. 3G, a nearly 50% decrease in A549 cell viability was found in $Lipo_{pCas9/gCDK4}$ and $LNT@Lipo_{pCas9/gCDK4}$ groups after treatment for 24 hours. When upon the addition of $LNT@Lipo_{pCas9/gCDK4}$ for 48 hours, the ratio of dead cells exceeded 90%. For comparison, the viability of H226 cells carrying wild-type KRAS slightly decreased after treatment with $LNT@Lipo_{pCas9/gCDK4}$ (Fig. 3H). In addition, the clone formation assay demonstrated an inhibition in the proliferation of KRAS-mutant tumor cells but not in wild-type KRAS tumor cells (Fig. 3I). Cell cycle suggested an exacerbated G_1/S arrest after cocultured with $Lipo_{pCas9/gCDK4}$ and $LNT@Lipo_{pCas9/gCDK4}$ for 24 hours as assessed by flow cytometry (Fig. 3J).

Lung tumor targeting of $LNT@Lipo_{pCas9/gCDK4}$ and CDK4 disruption in vivo

We mixed the $LNT@Lipo_{pCas9/gCDK4}$ with blood and measured the retention of the $Lipo_{pCas9/gCDK4}$ on the LNT cells after incubation for different times to investigate the stability of $LNT@Lipo_{pCas9/gCDK4}$ in the physiological condition. As depicted in fig. S6, a majority of LNT

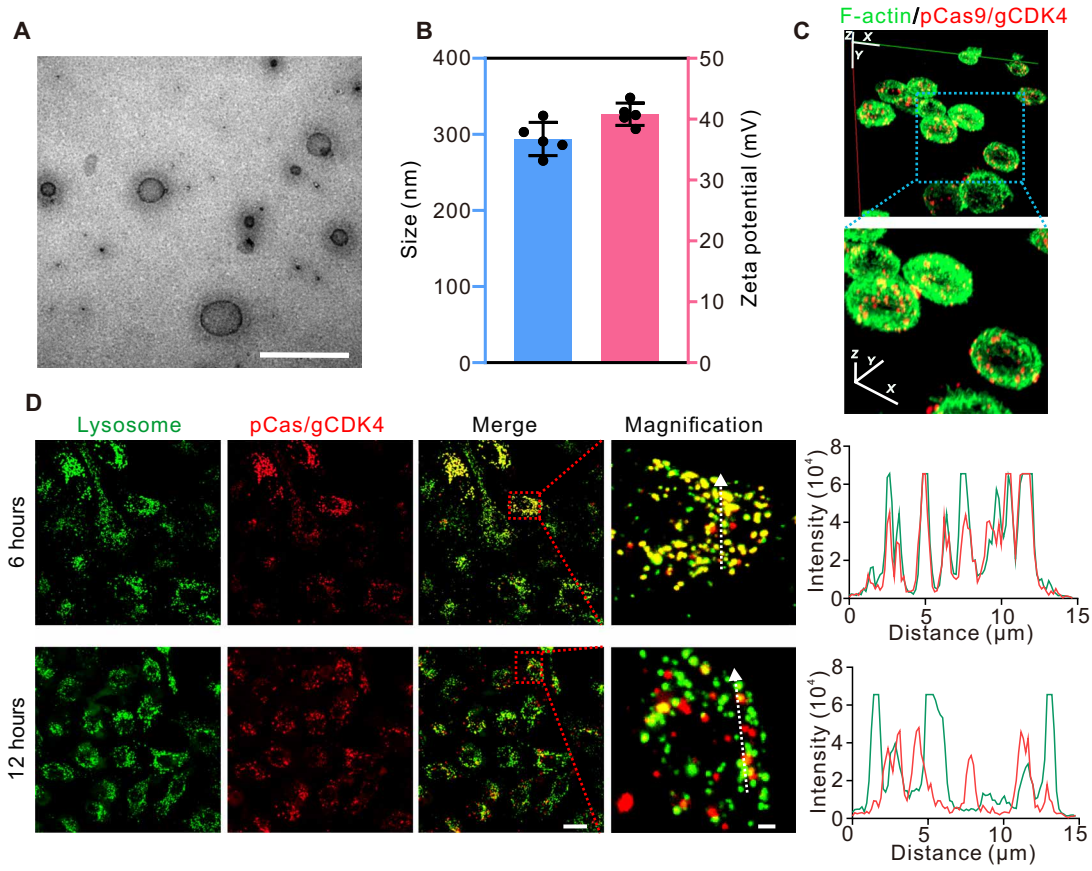

Fig. 2. Characterization of LNT@Lipo$_{pCas9/gCDK4}$. (**A**) Representative TEM image of lipofectamine nanoparticles encapsulating pCas9/gCDK4 plasmid. Scale bar, 1 μm. (**B**) Diameters and zeta potential of Lipo$_{pCas9/gCDK4}$ nanoparticles. $n = 5$. (**C**) Representative three-dimensional confocal images of Lipo$_{pCas9/gCDK4}$-loaded LNT A549 cells. F-actin was stained with phalloidin (green), and the pCas9/CDK4 plasmid was labeled with iFluor 647 (red). The scale bars of the top figure: 20 μm (*X* axis), 20 μm (*Y* axis), and 8 μm (*Z* axis). The scale bars of the bottom figure: 10 μm (*X* axis), 10 μm (*Y* axis), and 4 μm (*Z* axis). (**D**) Representative confocal images of localization of pCas9/gCDK4 plasmid in A549 cells after coculture with LNT@Lipo$_{pCas9/gCDK4}$ for different times, and white arrows indicate the colocalization analysis of pCas9/gCDK4 plasmid with lysosome. Lysosome was marked with LysoTracker Green, and pCas9/CDK4 plasmid was labeled with iFluor 647. Scale bars, 20 μm and 2 μm (enlarged view). Data are presented as means ± SD.

cells carried Lipo$_{pCas9/gCDK4}$, indicating a stable interaction between LNT cells and Lipo$_{pCas9/gCDK4}$. Next, we investigated the pharmacokinetics of LNT cells and Lipo$_{pCas9/gCDK4}$ after intravenous injection of LNT@Lipo$_{pCas9/gCDK4}$. As a result, we observed a similar pharmacokinetic curve in Lipo$_{pCas9/gCDK4}$ group compared with that in LNT cells group (fig. S7), indicating a synchronized clearance of LNT cells and Lipo$_{pCas9/gCDK4}$.

Tumor cells dispersed into the circulatory system tend toward micron-level dimension pulmonary capillary retention and enhanced tumor cell affinity (*38*). We hypothesized that LNT cells could effectively retained in the tumor foci and delivered the Lipo$_{pCas9/gCDK4}$ plasmids to the tumor cells. 1,1′-Dioctadecyl-3,3,3′,3′-tetramethylindodicarbocyanine,4-chlorobenzenesulfonate salt (DiD) was used to label lipofectamine for facilitating real-time observation of LNT@Lipo$_{pCas9/gCDK4}$ in vivo. Fluorescence imaging revealed more LNT@Lipo$_{pCas9/gCDK4}$ accumulation in the lungs within 16 hours compared with the mice receiving Lipo$_{pCas9/gCDK4}$. The attenuation of partial lung fluorescence could be due to the clearance of LNT cells by bloodstream within 24 hours (Fig. 4A). Furthermore, ex vivo image of lungs revealed stronger fluorescence signals in mice injected with LNT@Lipo$_{pCas9/gCDK4}$ with levels nearly fourfold higher than those treated with Lipo$_{pCas9/gCDK4}$ upon intravenous infusion for 6 hours (Fig. 4, B and C). The fluorescence signals of LNT@Lipo$_{pCas9/gCDK4}$ distributed in other major organs were also slightly higher as compared to Lipo$_{pCas9/gCDK4}$ group (fig. S8). Pathological fluorescence staining implied that the accumulation of LNT@Lipo$_{pCas9/gCDK4}$ in lungs was increased nearly 10-fold when receiving the injection of LNT@Lipo$_{pCas9/gCDK4}$ (Fig. 4, D and E). To investigate whether CD44 blocking affects the targeting efficiency of LNT@Lipo$_{pCas9/gCDK4}$, we used in vivo image system (IVIS) to observe the lungs of NSCLC-bearing mice after injecting Hermes-1 (CD44 blockage) pretreated LNT@Lipo$_{pCas9/gCDK4}$ for 8 hours. The IVIS images revealed reduced fluorescence intensity in the lungs following CD44 blocking (fig. S9), suggesting an inhibition of tumor-targeting ability in LNT cells. To assess the editing efficiency of pCas9/gCDK4 delivered by LNT@Lipo$_{pCas9/gCDK4}$, an immunofluorescent staining was conducted to visualize CDK4 expression in tumor lesions. A decreased expression was observed in LNT@Lipo$_{pCas9/gCDK4}$-treated samples compared to Lipo$_{pCas9/gCDK4}$ and other groups (Fig. 4F). Furthermore, Western blot analysis demonstrated a notable reduction in CDK4 protein levels within tumor nodules for LNT@Lipo$_{pCas9/gCDK4}$ treatment (Fig. 4, G and H).

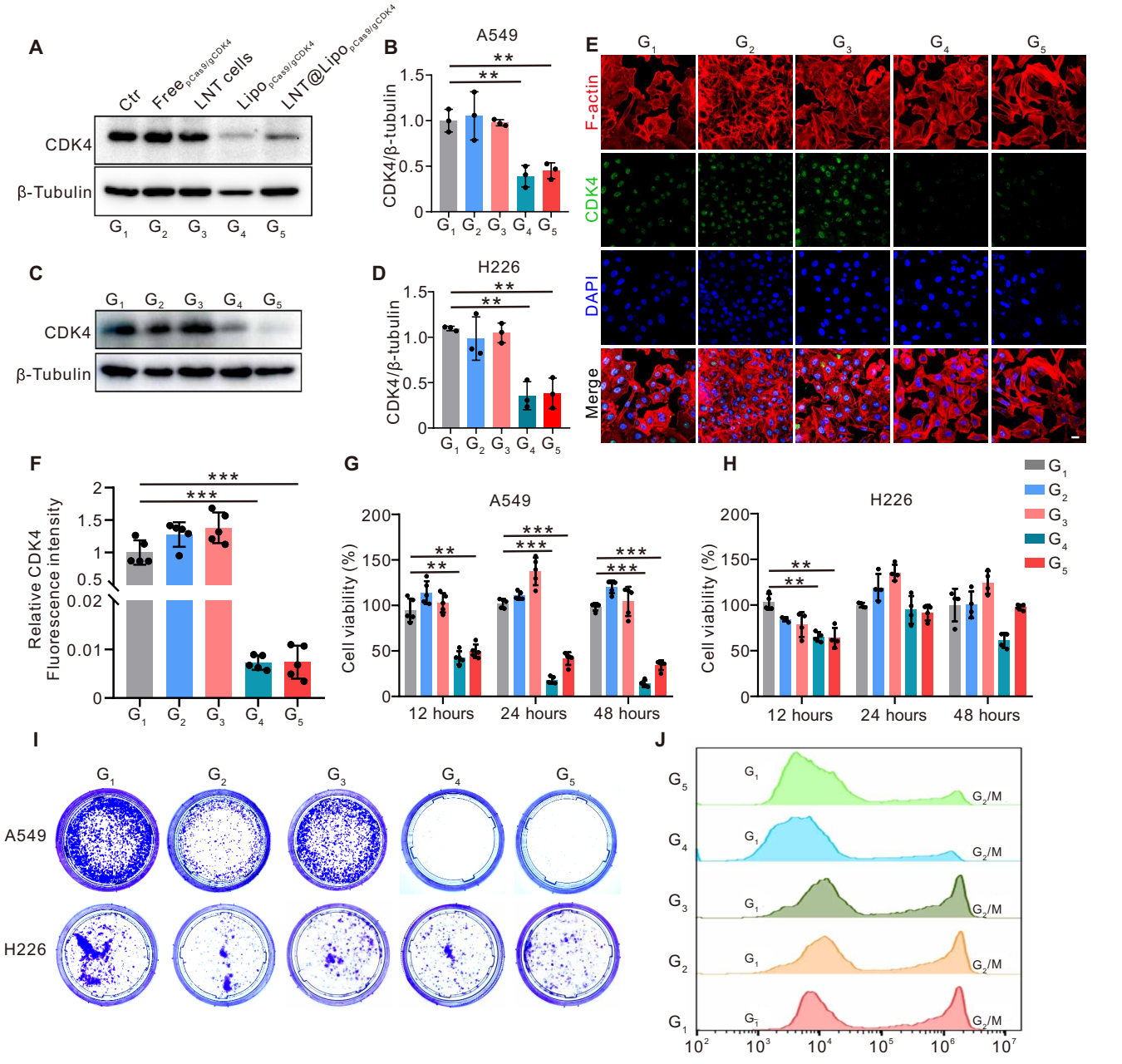

Fig. 3. Gene editing and antitumor efficacy of LNT@Lipo$_{pCas9/gCDK4}$ in vitro. (**A**) Western blot analysis of CDK4 in A549 cells (mutant KRAS) after treatment with PBS (Ctr) (G_1), free$_{pCas9/gCDK4}$ (G_2), LNT cells (G_3), Lipo$_{pCas9/gCDK4}$ (G_4), and LNT@Lipo$_{pCas9/gCDK4}$ (G_5) for 36 hours. (**B**) Statistics of protein expression intensity of CDK4 in A549 cells, $n = 3$. (**C**) Western blot analysis of CDK4 in H226 (wild-type KRAS) cells. (**D**) Statistics of CDK4 protein expression intensity in H226 cells, $n = 3$. (**E**) Representative confocal images of CDK4 expression in A549 cells after coincubation with LNT@Lipo$_{pCas9/gCDK4}$. CDK4 was fluorescently stained green; F-actin was fluorescently labeled red, nuclei were labeled with DAPI (blue). Scale bar, 20 μm. (**F**) Statistics of fluorescence intensity of CDK4 in A549 cells, $n = 5$. (**G**) Cell viability of A549 cells measured by CCK8 assay after treatment with LNT@Lipo$_{pCas9/gCDK4}$ for different times, $n = 5$. (**H**) Cell viability of H226 cells measured by CCK8 assay after treatment with LNT@Lipo$_{pCas9/gCDK4}$ for different times, $n = 4$. (**I**) Colony formation assay after treatment with LNT@Lipo$_{pCas9/gCDK4}$. (**J**) Cell cycle assay of A549 cells detected by flow cytometry after treatment with LNT@Lipo$_{pCas9/gCDK4}$. All data are presented as means ± SD. (B, D, and F to H). Statistical significance is calculated via ordinary one-way analysis of variance (ANOVA) (B, D, F, G, and H), $^{**}P < 0.01$, $^{***}P < 0.001$.

Regression of KRAS-mutant NSCLCs by LNT@Lipo$_{pCas9/gCDK4}$

To further explore the therapeutic effects of LNT@Lipo$_{pCas9/gCDK4}$ on pulmonary tumors, phosphate-buffered saline (PBS), free pCas9/gCDK4 plasmids, LNT A549 cells, Lipo$_{pCas9/gCDK4}$ nanoparticles, and LNT@Lipo$_{pCas9/gCDK4}$ were intravenously injected (Fig. 5A). The real-time bioluminescence signals of A549 cells were recorded by in vivo imaging system to monitor the growth kinetics of lung tumors in vivo. An obvious tumor regression was found in mice that received LNT@Lipo$_{pCas9/gCDK4}$ injection. Notably, 50% of tumor bioluminescence signals in mice receiving LNT@Lipo$_{pCas9/gCDK4}$ treatment were barely detectable 15 days after treatment. By contraries, the tumor bioluminescence signals in mice receiving the treatment of PBS, free pCas9/

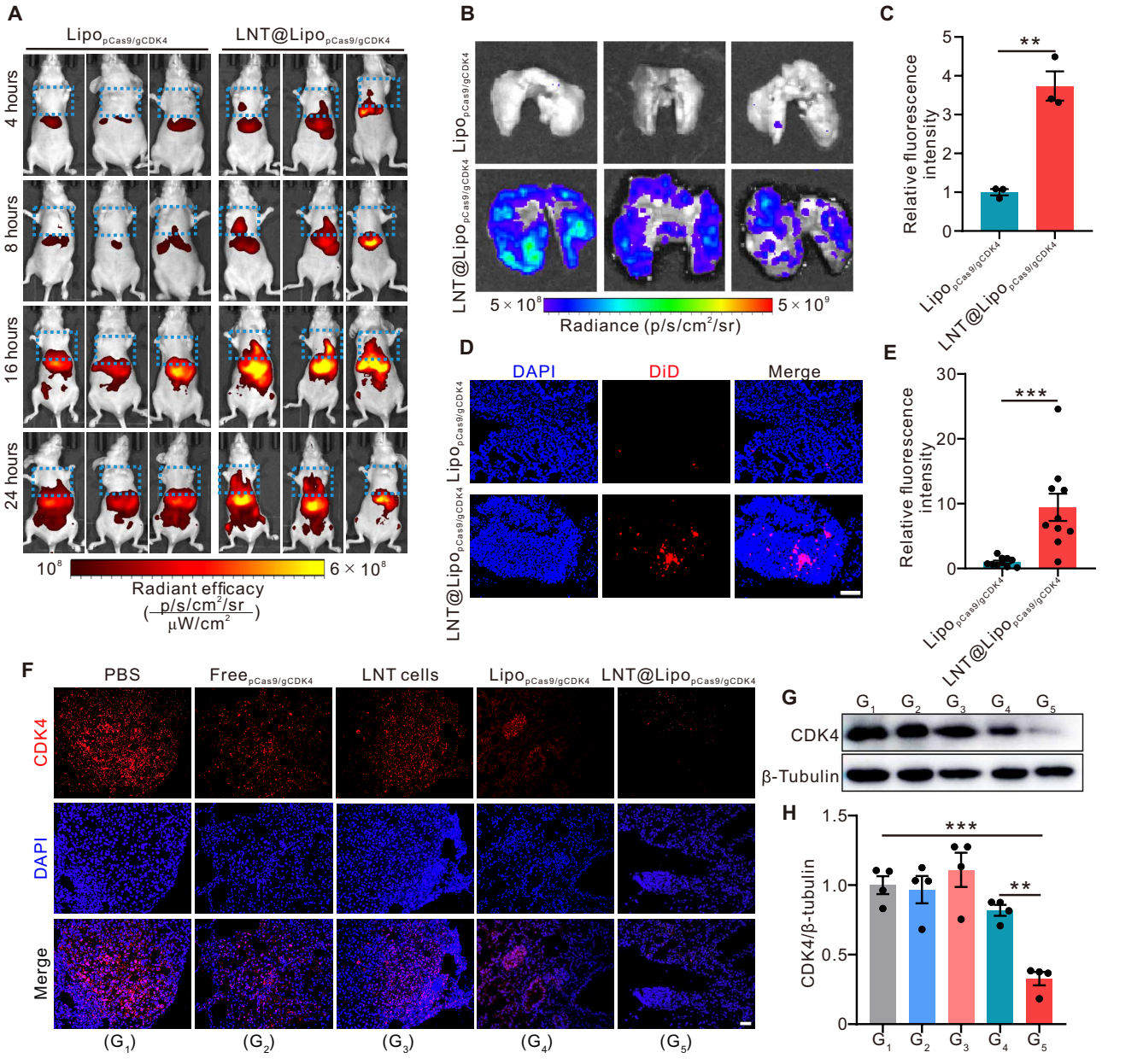

Fig. 4. Distribution and genome editing efficacy of LNT@Lipo$_{pCas9/gCDK4}$ in vivo. (**A**) Fluorescence images of DiD-labeled Lipo$_{pCas9/gCDK4}$ and LNT@Lipo$_{pCas9/gCDK4}$ distribution in A549 NSCLC carcinoma, $n = 3$. Blue dotted frames marked thorax. (**B**) Fluorescence images of isolated lungs after treatment with DiD-labeled Lipo$_{pCas9/gCDK4}$ and LNT@Lipo$_{pCas9/gCDK4}$ for 6 hours. (**C**) Statistics of isolated lung fluorescence intensity, $n = 3$. (**D**) Representative confocal images of Lipo$_{pCas9/gCDK4}$ distribution within lung tumors. Lipo$_{pCas9/gCDK4}$ was labeled with DiD (red); nuclei were labeled with DAPI (blue). Scale bar, 50 μm. (**E**) Statistics of fluorescence intensity of Lipo$_{pCas9/gCDK4}$ in tumor lesions, $n = 10$. (**F**) Representative immunofluorescence images of CDK4 in tumor lesions after treatment with PBS (G_1), free$_{pCas9/gCDK4}$ (G_2), LNT cells (G_3), Lipo$_{pCas9/gCDK4}$ (G_4), and LNT@Lipo$_{pCas9/gCDK4}$ (G_5) for 48 hours. CDK4 was stained with red; nuclei were labeled with DAPI (blue). Scale bar, 50 μm. (**G**) Western blot assay of CDK4 protein expression in tumor lesions. (**H**) Statistics of protein intensity of CDK4 in tumor lesions, $n = 4$. All data are presented as means ± SEM. (C, E, and H). Statistical significance is calculated via ordinary one-way ANOVA (H), and statistical significance is evaluated by unpaired *t* test (C and E), $^{**}P < 0.01$, $^{***}P < 0.001$.

gCDK4 plasmids, A549 LNT cells, and Lipo$_{pCas9/gCDK4}$ nanoparticles exhibited sustainable increase, and a rapid tumor progression could be observed (Fig. 5, B and C). In addition, no abnormal changes in body weight of tumor-bearing mice were observed during the treatment session (fig. S10), suggesting the safety of the therapeutic strategy.

To intuitively evaluate the therapeutic effect, we conducted hematoxylin and eosin (H&E) staining and obtained images of pulmonary tumor nodules. As shown in Fig. 5 (D and E), LNT@Lipo$_{pCas9/gCDK4}$ reduced the number of tumor nodules at the treatment endpoint, which was consistent with bioluminescence imaging. Moreover, 60% of the mice receiving treatment with LNT@Lipo$_{pCas9/gCDK4}$ survived for 100 days; comparatively, all PBS treated mice died within 70 days (Fig. 5F). To further verify the proliferation of the KRAS-mutant lung tumors, we performed Ki67 fluorescence staining after twice

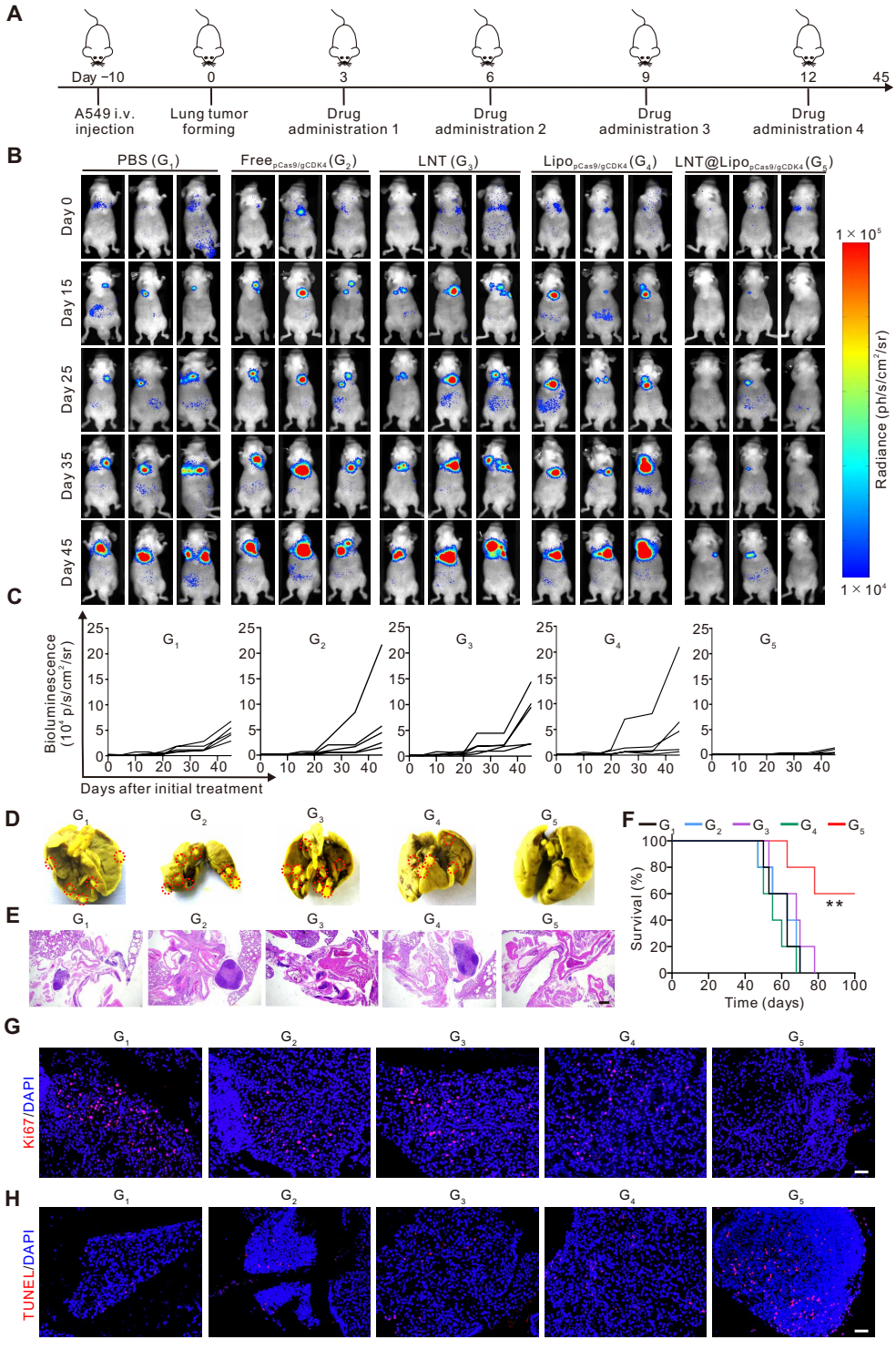

Fig. 5. Regression of tumor growth in vivo by LNT@Lipo$_{pCas9/gCDK4}$. (**A**) Schedule of the A549 in situ NSCLC models and treatment. (**B**) Representative bioluminescence images of tumor in vivo after injection with PBS (G_1), free$_{pCas9/gCDK4}$ (G_2), LNT cells (G_3), Lipo$_{pCas9/gCDK4}$ (G_4), and LNT@Lipo$_{pCas9/gCDK4}$ (G_5). (**C**) Tumor growth kinetics in different groups indicated by bioluminescence intensity, $n = 5$. (**D**) Representative lung photographs in different groups; red dotted circle marked tumors. (**E**) Representative H&E images of tumor lesions in different groups. Scale bar, 200 μm. (**F**) Survival rates of mice in different groups, $n = 5$. (**G**) Representative immunofluorescence images of Ki67 in tumor lesions of the mice after twice treatments. Ki67 was stained with red; nuclei were labeled with DAPI (blue). Scale bar, 50 μm. (**H**) Representative fluorescence images of TUNEL within the lung of the mice after twice treatments. TUNEL was stained with red; nuclei were labeled with DAPI. Scale bar, 50 μm. Statistical significance is calculated via log-rank (Mantel-Cox) test, $^{**}P < 0.01$.

administration. An obvious decrease in the Ki67 protein levels was observed in mice with LNT@Lipo$_{pCas9/gCDK4}$ treatment, compared with that in Lipo$_{pCas9/gCDK4}$ nanoparticle group (Fig. 5G). In addition, terminal deoxynucleotidyl transferase–mediated deoxyuridine triphosphate nick end labeling (TUNEL) staining revealed almost no fluorescent signal in free pCas9/gCDK4 plasmids, A549 LNT cells, and Lipo$_{pCas9/gCDK4}$ nanoparticle groups, However, a notable increase in apoptotic cells was found after treatment with LNT@Lipo$_{pCas9/gCDK4}$ (Fig. 5H).

To assess the biosafety of the LNT cells, Lipo$_{pCas9/gCDK4}$ and LNT@Lipo$_{pCas9/gCDK4}$, blood cells and serum biochemical analysis were conducted to evaluate any toxic effects after 1 and 3 days of treatment. As shown in fig. S11 (A and B), LNT cell treatment induced an increase in lymphocytes and monocytes, possibly due to LNT cell disintegration triggering an immune response on the first day. Moreover, Lipo$_{pCas9/gCDK4}$ led to a decrease in all white blood cells, including lymphocytes, neutrophils, and monocytes. It is worth to note that all these cell types had recovered to normal levels at 3 days posttreatment (fig. S11B). Similarly, the levels of alanine aminotransferase (ALT) and total bilirubin (TBIL) were elevated after injection with Lipo$_{pCas9/gCDK4}$ due to its own toxicity (fig. S11C). After 3 days of treatment, a high ALT level was maintained in the Lipo$_{pCas9/gCDK4}$ group, indicating that Lipo$_{pCas9/gCDK4}$ may result in liver injury (fig. S11D). By contrast, LNT@Lipo$_{pCas9/gCDK4}$ injection had no effects on the levels of ALT and TBIL. Furthermore, pathological evaluation of major organs showed no obvious pathological alteration as demonstrated by H&E staining (fig. S12).

DISCUSSION

In this study, we applied cryo-shocking tumor cells as gene targeting carriers for CDK4 genetic editing to induce synthetic lethal of KRAS-mutant of NSCLC. CDK4 is a critical mediator of G_1/S transition and contributes to the occurrence and malignancy of many tumor types (*39*). Certain studies have demonstrated the synthetic lethal interaction between CDK4 and KRAS, revealing that CDK4 presents a promising candidate for KRAS-mutant NSCLC therapy. To date, CRISPR-Cas9 harbors the distinct advantage for the treatment of various tumors by permanently disrupting crucial genes related to tumor survival and bypassing the repetitive dosing. Despite main gene delivery vehicles like virus and lipid nanoparticles hold high gene editing efficiency, challenges associated with immunogenicity, off-target gene effects, and dose-limiting toxicity hinder the further application in vivo (*17*, *40*–*42*). Compared with these exogenous and synthetic gene vectors, cell-based carriers exhibit excellent targeting capabilities due to the homologous protein components. However, some living cell types may have potential physiological toxicity or pathogenicity, restricting their clinical application. Our data support that rapid immersion in liquid nitrogen not only maintains the integrity of the cell structure but also inactivates tumor cells, eliminating potential pathogenicity. Preservation of the functional protein pool of LNT cells boosts lung active targeting ability by interacting with endothelial cells. Moreover, homologous receptors on LNT cells may also increase the probability of interaction with tumor cells and thus enhance the homologous targeting and efficiency of drug delivery. Compared with cell-deprived vesicles, physical size of LNT cells makes this CRISPR-Cas9 delivery system inclined to be captured by pulmonary capillaries, enhancing pulmonary retention.

Our data demonstrate the elevation of lymphocytes and monocytes after injection with LNT cells. This could be the reason that the release of intracellular nucleic acid and protein triggered immune response due to the disintegration of LNT cells. Moreover, liquid nitrogen shocking preserves the tumor antigens in LNT cells, supporting that the LNT cell could be a vaccine candidate for tumor immunotherapy. This suggests that LNT cells could be the carriers for delivering immunomodulatory drugs. In addition, LNT cells obtained from postoperative resection or needle biopsy enable the reuse of abandoned tumors. Liquid nitrogen shocking and the preparation procedure based on electrostatic anchoring are also feasible for large-scale preparation.

MATERIALS AND METHODS

Materials, cell lines, and animals

Lipofectamine 3000 was bought from Thermo Fisher Scientific (L3000015). The cryopreservation medium (NCRC-10001-50) was purchased from Cyagen Biosciences. CDK4 CRISPR-Cas9 knockout plasmid (sc-400148) was purchased from Santa Cruz. Actin-Tracker Green-488 (C2201S) was bought from Beyotime Biotechnology. Lentivirus expressing luciferase was purchased from HANBIO. A TUNEL assay kit (Red AF647) was obtained from Procell. Picogreen was purchased from Yeasen Biotechnology. A549 and H226 cell lines were obtained from the American Type Culture Collection. A549 and H226 cell lines were cultured in F12K medium and RPMI 1640 medium, which contain 10% fetal bovine serum and penicillin/streptomycin (100 U ml^{-1}; Biosharp) at 37°C in 5% CO_2. Five-week BALB/c nude mice (female/male) were obtained from Zhejiang Vital River Laboratory Animal Technology. Mouse study was conducted in accordance with the protocol approved by Animal Ethics Committee of Zhejiang University (ZJU20230329).

Preparation and characterization of LNT cells

A549 cells and H226 cells were harvested and dispersed in the cryopreservation medium with a density of 5×10^6/ml. The cellular medium was subsequently submerged in liquid nitrogen for a period of 12 hours. Before use, the liquid nitrogen–treated cells were thawed in an ice bath and lastly resuspended at 37°C, pelleted at 500*g* for 3 min and washed once with PBS.

To observe the structure, LNT cells were stained with 4′,6-diamidino-2-phenylindole (DAPI) and AF488-conjugated phalloidin. Briefly, 1×10^6 LNT cells were fixed with paraformaldehyde for 10 min. Then, the cells were suspended in 500 μl of PBS containing phalloidin stock solution (6.6 μM) for 20 min. Then, the cells were collected under the centrifugation with 500*g* for 3 min. After that, PBS with DAPI (1 μg/ml) was used to label the nucleus. The cells were suspended in PBS and observed by confocal microscopy (Zeiss LSM 800).

For cell structure analysis, LNT cells were fixed in 2.5% glutaraldehyde for 30 min. Afterward, graded ethanol (30, 50, 70, 85, and 90%) were used to dehydrate for 10 min and 100% ethanol was utilized to wash twice for 30 min. The dehydrated LNT cells then were dropped on silicon wafer and further analyzed by SEM (Nova Nano 450).

For cell viability analysis, LNT A549 cells were treated with 2 μM calcein-AM and 0.5 μM propidium iodide for 30 min at 37°C and were analyzed by a laser scanning confocal microscope (LSCM). Moreover, CCK8 was performed to evaluate the viability after cryo-shocking with liquid nitrogen.

Preparation and characterization of LNT@Lipo$_{pCas9/gCDK4}$

Lipofectamine 3000–pCas9/gCDK4 nanoparticles (Lipo$_{pCas9/gCDK4}$) were prepared according to the manufacturer's instructions (Thermo Fisher Scientific). To obtain LNT@Lipo$_{pCas9/gCDK4}$, Lipo$_{pCas9/gCDK4}$ were cocultured with LNT cells at 37°C for 1 hour and collected after centrifugation with 500*g* for 3 min. To facilitate visual observation, we labeled plasmid with PHOTOPROBE Biotin Reagents (SP-1000, Vector Laboratories) and then incubated them with iFluor 647–streptavidin conjugate. We cocultured LNT cells with iFluor 647–labeled pCas9/gCDK4 plasmid for 1 hour to obtain LNT@Lipo$_{pCas9/gCDK4}$. Then, the cells were stained with F-actin for 40 min and observed with LSCM.

Colocalization of LNT@Lipo$_{pCas9/gCDK4}$ with lysosome

To analyze the escape ability from the lysosome, we cocultured iFluor 647–labeled LNT@Lipo$_{pCas9/gCDK4}$ with A549 cells for the appointed time (1, 2, 4, 6, 8, and 12 hours). After that, we used PBS to wash the cells and stained with lysosome tracker green 488 for 40 min. Then, the cell was washed with PBS and analyzed with LCSM.

Loading and releasing of Lipo$_{pCas9/gCDK4}$ from LNT A549 cells

To load Lipo$_{pCas9/gCDK4}$, the pCas9/gCDK4 plasmid was labeled with Picogreen at a ratio of 1000 μl of working solution per 2 μg plasmid (YEASEN, 12641ES01). The labeled plasmid underwent filtration with a hyperfiltration tube at 4000 rpm for 15 min, followed by two washes with PBS. Subsequently, varying doses (2, 4, 6, 8, 10, and 12 μg) of Picogreen-labeled plasmid were used to prepare Lipo$_{pCas9/gCDK4}$. This Lipo$_{pCas9/gCDK4}$ was then cocultured with 2.5×10^6 LNT cells for 1 hour to obtain LNT@Lipo$_{pCas9/gCDK4}$. The collected LNT@Lipo$_{pCas9/gCDK4}$ was obtained by centrifugation at 500*g* for 5 min, followed by lysis in PBS containing 2% Triton X-100 for 20 min. Fluorescence intensity at Excitation (Ex): 490 nm/Emission (Em): 520 nm was measured using a microplate reader.

For the releasing of Lipo$_{pCas9/gCDK4}$, Lipo$_{pCas9/gCDK4}$ nanoparticles containing 10 μg of iFluor 647–streptavidin–conjugated pCas9/gCDK4 plasmid were loaded to 2.5×10^6 LNT A549 cells. After that, the LNT@Lipo$_{pCas9/gCDK4}$ was incubated at 37°C, 100 rpm/min for different times (0, 1, 2, 4, 6, 8, and 10 hours). At the appointed time, the supernatant containing fluorescent-labeled plasmids was centrifuged and collected. The fluorescence intensity was detected by microplate reader at Ex 635 nm/Em 660 nm.

Cell viability analysis after treatment with LNT@Lipo$_{pCas9/gCDK4}$

A549 cells were seeded in 96-well plates at 5×10^3 cells per well. After 24 hours, cells were treated with PBS, pCas9/gCDK4, LNT cells, Lipo$_{pCas9/gCDK4}$, and LNT@Lipo$_{pCas9/gCDK4}$ (containing 0.2 μg plasmid per well) for different times (12, 24, and 48 hours). CCK8 assay was carried out for evaluating cell viability by a microplate reader at optical density of 450 nm.

For cell proliferation analysis, A549 cells were seeded in 24-well plates at 5×10^4 cells per well and treated with PBS, pCas9/gCDK4, LNT cells, Lipo$_{pCas9/gCDK4}$, and LNT@Lipo$_{pCas9/gCDK4}$ (containing 0.5 μg plasmid per well). After 24 hours, 1×10^3 cells were digested and planted into 35-mm petri dish, respectively. After 10 days, cells were fixed with methanol and stained with crystal violet for 60 min. To further evaluate the cell proliferation ability after treatment with LNT@Lipo$_{pCas9/gCDK4}$, we seeded A549 cells in six-well plates with the density of 5×10^5 cells per well and received the treatment with PBS, pCas9/gCDK4, LNT cells, Lipo$_{pCas9/gCDK4}$, and LNT@Lipo$_{pCas9/gCDK4}$ (5×10^5 LNT cells loaded with 2.5 μg of plasmid per well) for 24 hours. 5-Ethynyl-2′-deoxyuridine staining was carried out and analyzed by flow cytometry.

LNT@$_{LipopCas9/gCDK4}$ accumulation in lung tumors

We initiated the construction of KRAS-mutant NSCLCs by intravenously injecting 2×10^6 A549 cells. After 30 days, mice were divided into two groups ($n = 3$) and intravenously injected with DiD-labeled Lipo$_{pCas9/gCDK4}$ and LNT@Lipo$_{pCas9/gCDK4}$, respectively. The in vivo distribution was monitored at 4, 6, 8, 16, and 24 hours using an imaging system (IVIS). DiD signals were observed ex vivo in the collected lungs through IVIS. For histological analysis, lung sections were examined under a confocal microscope after staining the nucleus with DAPI.

LNT was labeled with cell tracker red CMTPX dye before immersion in liquid nitrogen. After thawed, LNT cells were incubated with human CD44 blockage Hermes-1 (Thermo Fisher Scientific) for 1 hour at 37°C. Then, NSCLC-bearing mice were intravenously injected with labeled LNT@Lipo$_{pCas9/gCDK4}$. After 8 hours, we euthanized the mice and collected the lungs and monitored the fluorescence signal by IVIS.

Pharmacokinetics and stability analysis of LNT@$_{LipopCas9/gCDK4}$ in blood

We used cell tracker orange to label LNT cells and iFluor 647 to label pCas9/gCDK4 plasmid for preparing dual-color labeling LNT@$_{LipopCas9/gCDK4}$. Dual-color labeling LNT@$_{LipopCas9/gCDK4}$ was intravenously injected, and the blood was collected at different times. IVIS was used to analyze the fluorescence intensity and calculate the percentage of injected dose (% ID).

For stability analysis of LNT@Lipo$_{pCas9/gCDK4}$ in blood, dual-color labeling LNT@$_{LipopCas9/gCDK4}$ (containing 1.5×10^5 LNT cells) was mixed with 100 μl of blood for different times. At the appointed time, the whole blood was fixed with paraformaldehyde, and subjected to flow cytometry analysis.

In vivo treatment of KRAS-mutant NSCLC

To evaluate the therapeutic effect, we intravenously injected 2×10^6 A549 cells to establish KRAS-mutant NSCLC models. At day 10, PBS, free$_{pCas9/gCDK4}$, LNT cells, Lipo$_{pCas9/gCDK4}$, and LNT@Lipo$_{pCas9/gCDK4}$ (2.5×10^6 LNT cells) (all of the treatment groups contained 10 μg of plasmid) were administrated intravenously per mouse every 3 days for four times. To observe the growth kinetics of tumors, bioluminescence signals of mice were captured in every group every 5 days. On day 50, mice were euthanized for observation of tumor growth in the lungs. The lung tissues bearing NSCLC were fixed with Bouin's fluid to evaluate the tumor nodules in lungs or paraformaldehyde (4%) solution for H&E staining to analyze the tumor lesions on the lungs.

Editing efficacy of CDK4 in vitro and in vivo

A549 and H226 cells were planted into six-well plates and then received the treatment of PBS, free$_{pCas9/gCDK4}$, LNT cells, Lipo$_{pCas9/gCDK4}$, and LNT@Lipo$_{pCas9/gCDK4}$ (2.5 μg pCas9/gCDK4 plasmid) for 36 hours. Cells were lysed by using radio immunoprecipitation assay (RIPA, P0013B, Beyotime) with 10 μM phenylmethylsulfonyl fluoride (PMSF; ST507, Beyotime) to obtain total protein and were performed with Western blot assay according to the CDK4 primary antibody (1:1000; 11026-1-AP, Proteintech). After treated with PBS,

free$_{pCas9/gCDK4}$, LNT cells, Lipo$_{pCas9/gCDK4}$, and LNT@Lipo$_{pCas9/gCDK4}$ twice, lung tumor tissues were collected and lysed with RAPI containing 10 μM PMSF. After that, we performed Western blot assay to evaluate the editing efficacy of LNT@Lipo$_{pCas9/gCDK4}$. The CDK4 protein expression levels were analyzed by ImageJ software. All the blot original images in Western blot analyses were shown in fig. S13.

Immunofluorescence staining

A549 lung tumor tissues were obtained from the mice after treatment and embedded with paraffin before sectioning into 4 μm. Before staining, the tissues were dewaxed and microwave was used to repair antigens. A total of 0.5% Triton X-100 and 1% bovine serum albumin were used to permeabilize and block the nonspecific binding. CDK4 was labeled with CDK4 primary antibody (1:200; 11026-1-AP, Proteintech) and marked with Alexa Fluor 647–conjugated second antibody (1:500; ab150075, Abcam). After that, the nuclei were stained with DAPI. Ki67 primary antibody (1:200; AF0198, Affinity) was used to detect the expression of Ki67 for evaluating the proliferation of tumors in lungs. For analyzing the apoptosis of tumor cells, TUNEL staining was carried out, and the 3'-oxhydryl (3-OH) terminal of fragmented DNA was labeled with red. In addition, the nuclear in all tumor slides were stained with DAPI. All the stained slides were observed by a ZEISS fluorescence microscope (Axio Observer 7), and the fluorescence intensity was analyzed with ImageJ software.

In vivo biocompatibility evaluation

Eight-week-old C57BL/6J mice were received treatment with PBS, free$_{pCas9/gCDK4}$, LNT cells, Lipo$_{pCas9/gCDK4}$, and LNT@Lipo$_{pCas9/gCDK4}$ containing 2.5 μg of pCas9/gCDK4 (intravenously) for 1 and 3 days. At the designated time point, we euthanized the mice and collected the blood plasma and serum for biochemical analysis. Major organ tissues were fixed with paraformaldehyde, and H&E staining was performed for pathological analysis.

Statistical analysis

All results were independently repeated at least three times and reported as means ± SD or mean ± SEM as specified. Student's *t* test was performed to compare the data between two groups. Tukey post hoc tests and one-way analysis of variance (ANOVA) were used for multiple comparisons. Survival curves were analyzed using the log-rank (Mantel-Cox) test. GraphPad Prism software was used to conduct all statistical analyses. A statistically significant difference was defined as $P < 0.05$.

Supplementary Materials

This PDF file includes:

Figs. S1 to S13

REFERENCES AND NOTES

1. H. Sung, J. Ferlay, R. L. Siegel, M. Laversanne, I. Soerjomataram, A. Jemal, F. Bray, Global Cancer Statistics 2020: GLOBOCAN estimates of incidence and mortality worldwide for 36 cancers in 185 countries. *CA Cancer J. Clin.* **71**, 209–249 (2021).
2. M. Wang, R. S. Herbst, C. Boshoff, Toward personalized treatment approaches for non-small-cell lung cancer. *Nat. Med.* **27**, 1345–1356 (2021).
3. R. S. Herbst, D. Morgensztern, C. Boshoff, The biology and management of non-small cell lung cancer. *Nature* **553**, 446–454 (2018).
4. H. Padinharayil, J. Varghese, M. C. John, G. K. Rajanikant, C. M. Wilson, M. Al-Yozbaki, K. Renu, S. Dewanjee, R. Sanyal, A. Dey, A. G. Mukherjee, U. R. Wanjari, A. V. Gopalakrishnan, A. George, Non-small cell lung carcinoma (NSCLC): Implications on molecular pathology and advances in early diagnostics and therapeutics. *Genes. Dis.* **10**, 960–989 (2023).
5. G. V. Scagliotti, P. Parikh, J. von Pawel, B. Biesma, J. Vansteenkiste, C. Manegold, P. Serwatowski, U. Gatzemeier, R. Digumarti, M. Zukin, J. S. Lee, A. Mellemgaard, K. Park, S. Patil, J. Rolski, T. Goksel, F. de Marinis, L. Simms, K. P. Sugarman, D. Gandara, Phase III study comparing cisplatin plus gemcitabine with cisplatin plus pemetrexed in chemotherapy-naive patients with advanced-stage non-small-cell lung cancer. *J. Clin. Oncol.* **26**, 3543–3551 (2008).
6. S. Gettinger, L. Horn, D. Jackman, D. Spigel, S. Antonia, M. Hellmann, J. Powderly, R. Heist, L. V. Sequist, D. C. Smith, P. Leming, W. J. Geese, D. Yoon, A. Li, J. Brahmer, Five-year follow-up of nivolumab in previously treated advanced non-small-cell lung cancer: Results from the CA209-003 study. *J. Clin. Oncol.* **36**, 1675–1684 (2018).
7. W. Zhong, X. Zhang, Y. Zeng, D. Lin, J. Wu, Recent applications and strategies in nanotechnology for lung diseases. *Nano Res.* **14**, 2067–2089 (2021).
8. Z. Xu, Q. Wang, H. Zhong, Y. Jiang, X. Shi, B. Yuan, N. Yu, S. Zhang, X. Yuan, S. Guo, Y. Yang, Carrier strategies boost the application of CRISPR/Cas system in gene therapy. *Exp. Dermatol.* **2**, 20210081 (2022).
9. C. Xu, Z. Lu, Y. Luo, Y. Liu, Z. Cao, S. Shen, H. Li, J. Liu, K. Chen, Z. Chen, X. Yang, Z. Gu, J. Wang, Targeting of NLRP3 inflammasome with gene editing for the amelioration of inflammatory diseases. *Nat. Commun.* **9**, 4092 (2018).
10. Z. Wang, K. Cui, U. Costabel, X. Zhang, Nanotechnology-facilitated vaccine development during the coronavirus disease 2019 (COVID-19) pandemic. *Exp. Dermatol.* **2**, 20210082 (2022).
11. W. Sun, J. Wang, Q. Hu, X. Zhou, A. Khademhosseini, Z. Gu, CRISPR-Cas12a delivery by DNA-mediated bioresponsive editing for cholesterol regulation. *Sci. Adv.* **6**, eaba2983 (2020).
12. S. W. Wang, C. Gao, Y. M. Zheng, L. Yi, J. C. Lu, X. Y. Huang, J. B. Cai, P. F. Zhang, Y. H. Cui, A. W. Ke, Current applications and future perspective of CRISPR/Cas9 gene editing in cancer. *Mol. Cancer* **21**, 57 (2022).
13. S. Hamis, P. Nithiarasu, G. G. Powathil, What does not kill a tumour may make it stronger: In silico insights into chemotherapeutic drug resistance. *J. Theo. Biol.* **454**, 253–267 (2018).
14. M. J. Mitchell, M. M. Billingsley, R. M. Haley, M. E. Wechsler, N. A. Peppas, R. Langer, Engineering precision nanoparticles for drug delivery. *Nat. Rev. Drug Discov.* **20**, 101–124 (2021).
15. H. Deng, W. Huang, Z. Zhang, Nanotechnology based CRISPR/Cas9 system delivery for genome editing: Progress and prospect. *Nano Res.* **12**, 2437–2450 (2019).
16. J. M. Crudele, J. S. Chamberlain, Cas9 immunity creates challenges for CRISPR gene editing therapies. *Nat. Commun.* **9**, 3497 (2018).
17. A. Raguram, S. Banskota, D. R. Liu, Therapeutic in vivo delivery of gene editing agents. *Cell* **185**, 2806–2827 (2022).
18. D. Rosenblum, A. Gutkin, R. Kedmi, S. Ramishetti, N. Veiga, A. M. Jacobi, M. S. Schubert, D. Friedmann-Morvinski, Z. R. Cohen, M. A. Behlke, J. Lieberman, D. Peer, CRISPR-Cas9 genome editing using targeted lipid nanoparticles for cancer therapy. *Sci. Adv.* **6**, eabc9450 (2020).
19. N. J. O'Neil, M. L. Bailey, P. Hieter, Synthetic lethality and cancer. *Nat. Rev. Genet.* **18**, 613–623 (2017).
20. K. Cheng, N. U. Nair, J. S. Lee, E. Ruppin, Synthetic lethality across normal tissues is strongly associated with cancer risk, onset, and tumor suppressor specificity. *Sci. Adv.* **7**, eabc2100 (2021).
21. C. J. Ryan, I. Mehta, N. Kebabci, D. J. Adams, Targeting synthetic lethal paralogs in cancer. *Trends Cancer* **9**, 397–409 (2023).
22. A. Huang, L. A. Garraway, A. Ashworth, B. Weber, Synthetic lethality as an engine for cancer drug target discovery. >*Nat. Rev. Drug Discov.* **19**, 23–38 (2020).
23. C. Kofink, N. Trainor, B. Mair, S. Wöhrle, M. Wurm, N. Mischerikow, M. J. Roy, G. Bader, P. Greb, G. Garavel, E. Diers, R. McLennan, C. Whitworth, V. Vetma, K. Rumpel, M. Scharnweber, J. E. Fuchs, T. Gerstberger, Y. Cui, G. Gremel, P. Chetta, S. Hopf, N. Budano, J. Rinnenthal, G. Gmaschitz, M. Mayer, M. Koegl, A. Ciulli, H. Weinstabl, W. Farnaby, A selective and orally bioavailable VHL-recruiting PROTAC achieves SMARCA2 degradation in vivo. >*Nat. Commun.* **13**, 5969 (2022).
24. N. Vasan, J. Baselga, D. M. Hyman, A view on drug resistance in cancer. *Nature* **575**, 299–309 (2019).
25. P. A. Jänne, G. J. Riely, S. M. Gadgeel, R. S. Heist, S.-H. I. Ou, J. M. Pacheco, M. L. Johnson, J. K. Sabari, K. Leventakos, E. Yau, L. Bazhenova, M. V. Negrao, N. A. Pennell, J. Zhang, K. Anderes, H. Der-Torossian, T. Kheoh, K. Velastegui, X. Yan, J. G. Christensen, R. C. Chao, A. I. Spira, Adagrasib in Non–Small-Cell Lung Cancer Harboring aKRASG12CMutation. >*N. Engl. J. Med.* **387**, 120–131 (2022).
26. C. J. Lord, A. Ashworth, PARP inhibitors: Synthetic lethality in the clinic. *Science* **355**, 1152–1158 (2017).
27. S. R. Punekar, V. Velcheti, B. G. Neel, K. K. Wong, The current state of the art and future trends in RAS-targeted cancer therapies. >*Nat. Rev. Clin. Oncol.* **19**, 637–655 (2022).
28. L. Huang, Z. Guo, F. Wang, L. Fu, KRAS mutation: From undruggable to druggable in cancer. >*Sig. Transduct. Target. Ther.* **6**, 386 (2021).

29. M. Puyol, A. Martin, P. Dubus, F. Mulero, P. Pizcueta, G. Khan, C. Guerra, D. Santamaria, M. Barbacid, A synthetic lethal interaction between K-Ras oncogenes and Cdk4 unveils a therapeutic strategy for non-small cell lung carcinoma. *Cancer Cell* **18**, 63–73 (2010).
30. L. Esteban-Burgos, H. Wang, P. Nieto, J. Zheng, C. Blanco-Aparicio, C. Varela, G. Gomez-Lopez, F. Fernandez-Garcia, M. Sanclemente, C. Guerra, M. Drosten, J. Galan, E. Caleiras, J. Martinez-Torrecuadrada, L. Fajas, S. B. Peng, D. Santamaria, M. Musteanu, M. Barbacid, Tumor regression and resistance mechanisms upon CDK4 and RAF1 inactivation in KRAS/P53 mutant lung adenocarcinomas. *Proc. Natl. Acad. Sci. U.S.A.* **117**, 24415–24426 (2020).
31. M. R. Kelly, K. Kostyrko, K. Han, N. A. Mooney, E. E. Jeng, K. Spees, P. T. Dinh, K. L. Abbott, D. M. Gwinn, E. A. Sweet-Cordero, M. C. Bassik, P. K. Jackson, Combined proteomic and genetic interaction mapping reveals new RAS effector pathways and susceptibilities. *Cancer Discov.* **10**, 1950–1967 (2020).
32. T. Ci, H. Li, G. Chen, Z. Wang, J. Wang, P. Abdou, Y. Tu, G. Dotti, Z. Gu, Cryo-shocked cancer cells for targeted drug delivery and vaccination. >*Sci. Adv.* **6**, (2020).
33. Q. Wu, H. Huang, M. Sun, R. Zhang, J. Wang, H. Zheng, C. Zhu, S. Yang, X. Shen, J. Shi, F. Liu, W. Wu, J. Sun, F. Liu, H. Li, Z. Gu, Inhibition of tumor metastasis by liquid-nitrogen-shocked tumor cells with oncolytic viruses infection. >*Adv. Mater.* **35**, 2212210 (2023).
34. G. S. Offeddu, C. Hajal, C. R. Foley, Z. Wan, L. Ibrahim, M. F. Coughlin, R. D. Kamm, The cancer glycocalyx mediates intravascular adhesion and extravasation during metastatic dissemination. >*Commun. Biol.* **4**, 255 (2021).
35. C. Chen, S. Zhao, A. Karnad, J. W. Freeman, The biology and role of CD44 in cancer progression: Therapeutic implications. >*J. Hematol. Oncol.* **11**, 64 (2018).
36. A. Katti, B. J. Diaz, C. M. Caragine, N. E. Sanjana, L. E. Dow, CRISPR in cancer biology and therapy. >*Nat. Rev. Cancer* **22**, 259–279 (2022).
37. N. Wang, C. Liu, Y. Li, D. Huang, X. Wu, X. Kou, X. Wang, Q. Wu, C. Gong, A cooperative nano-CRISPR scaffold potentiates immunotherapy via activation of tumour-intrinsic pyroptosis. >*Nat. Commun.* **14**, 779 (2023).
38. Z. Zhao, L. Fang, P. Xiao, X. Sun, L. Zhou, X. Liu, J. Wang, G. Wang, H. Cao, P. Zhang, Y. Jiang, D. Wang, Y. A.-O. Li, Walking dead tumor cells for targeted drug delivery against lung metastasis of triple-negative breast cancer. >*Adv. Mater.* **34**, 2205462 (2022).
39. S. Goel, J. S. Bergholz, J. J. Zhao, Targeting CDK4 and CDK6 in cancer. *Nat. Rev. Cancer* **22**, 356–372 (2022).
40. D. L. Wagner, L. Amini, D. J. Wendering, L. M. Burkhardt, L. Akyüz, P. Reinke, H.-D. Volk, M. Schmueck-Henneresse, High prevalence of Streptococcus pyogenes Cas9-reactive T cells within the adult human population. >*Nat. Med.* **25**, 242–248 (2019).
41. A. V. Anzalone, L. W. Koblan, D. R. Liu, Genome editing with CRISPR–Cas nucleases, base editors, transposases and prime editors. >*Nat. Biotech.* **38**, 824–844 (2020).
42. T. Wei, Q. Cheng, L. Farbiak, D. A. O. Anderson, R. A.-O. Langer, D. A.-O. Siegwart, Delivery of tissue-targeted scalpels: Opportunities and challenges for In Vivo CRISPR/Cas-Based genome editing. *ACS Nano* **14**, 9243–9262 (2020).

Acknowledgments: We thank Q. Han and G.Z. Zhu in the Center of Cryo-Electron Microscopy (CCEM) Zhejiang University for technical assistance on confocal laser scanning microscopy and scanning electron microscope. **Funding:** This work was supported by the National Key R&D Program of China (2021YFA0909900) and the National Natural Science Foundation of China (52233013) to Z.G., the National Natural Science Foundation of China (52173142) to H.L., the China Postdoctoral Science Foundation (2022 M712718) to F.L., the China Postdoctoral Science Foundation (2021 M700118) to T.L., and the grants from the Startup Package of Zhejiang University to Z.G. and H.L. **Author contributions:** Conceptualization: Z.G., H.L., and K.H. Methodology: F.L., M.X., H.F., W.Z., T.S., Q.W., Z.L., P.W., T.L., J.S., and R.Z. Validation: F.L., M.X., H.F., W.Z., T.S., Q.W., Z.L., P.W., T.L., J.S., and R.Z. Writing—original draft: F.L., M.X., Z.G., H.L., and K.H. Writing—review and editing: F.L., M.X., Z.G., H.L., and K.H.. **Competing interests:** Z.G. is the co-founder of Zenomics Inc., Zcapsule Inc., and μZen Inc. All other authors declare that they have no competing interests. **Data and materials availability:** All data needed to evaluate the conclusions in the paper are present in the paper and/or the Supplementary Materials. The source data are publicly available on Science Data Bank (https://scidb.cn/s/eMNvmy).

Submitted 14 September 2023
Accepted 23 February 2024
Published 29 March 2024
10.1126/sciadv.adk8264